IOP Conf. Series: Journal of Physics: Conf. Series **871** (2017) 012047 doi:10.1088/1742-6596/871/1/012047

Numerical reproduction of screening-current-induced fields in HTS tape windings using finite element method

Yuma Okabe, Tomokazu Honda and Kazuhiro Kajikawa

Department of Electrical and Electronic Engineering, Kyushu University, 744 Motooka, Nishi-ku, Fukuoka 819-0395, Japan

E-mail: okabe@sc.kyushu-u.ac.jp

Abstract. The screening-current-induced fields in one of the high temperature superconducting (HTS) coils fabricated previously with coated conductors are evaluated numerically by using a one-dimensional finite element method, in which only the perpendicular component of a current vector potential is considered due to a very thin superconductor layer in the coated conductor. It is assumed that the voltage-current characteristics in the superconductor layer can be expressed by the critical state or n-value model, in which the field-dependent critical current density is also taken into account. The numerically calculated results of the screening-current-induced fields are compared with the experimental results carried out previously.

1. Introduction

Superconducting magnets for magnetic resonance imaging and nuclear magnetic resonance require a highly uniform magnetic field in their central part, so that these magnets have been usually wound with multifilamentary wires composed of low temperature superconductors. On the other hand, high temperature superconducting (HTS) wires have also been developed and become commercially available, and these wires are in the form of a flat tape with very large cross-sectional aspect ratio. Therefore, if this type of wire is used as a winding for superconducting magnet and a transport current is applied to it, the central magnetic field has very low uniformity because of a screening current induced in the HTS tape [1]. In order to eliminate the screening-current-induced fields (SCFs), the methods based on the abnormal transverse-field effect [2–5] or vortex shaking effect [6–8] have been proposed and validated experimentally [9–11]. Although the theoretical expressions for the decays of magnetizations in a single superconductor (SC) strip have been derived [6–8], there has been no useful method to estimate the decay of SCF in an HTS coil during the application of a cyclic external magnetic field.

In this study, the SCFs in simplified models of an HTS coil are numerically calculated using a finite element method [1, 12]. The decays of SCFs due to applications of cyclic fields are also evaluated on the basis of the theoretical expression for single SC strip [7, 8]. Furthermore, the obtained numerical results are compared with experimental results carried out previously [11].

2. Modeling and calculation method

The specifications of the HTS tape and coil used in the previous experiments are listed in Tables 1 and 2, respectively [11]. The width w of tape and the thickness d of SC layer are 5.03 mm and 2.6 μm, respectively. The critical current I_{c0} at 77 K in self-field is 257 A. The fabricated HTS coil is composed of four double pancakes without any joint between them. The inner and outer diameters of coil are 66.0 mm

Table 1. Specifications of HTS tape [11].

Parameter	Value
Tape width (without insulator), w	5.03 mm
Tape thickness (without insulator)	0.159 mm
Thickness of SC layer, d	2.6 μm
Critical current at 77 K in self-field, I_{c0}	257 A

Table 2. Specifications of HTS coil [11].

Parameter	Value
Inner diameter	66.0 mm
Outer diameter	70.7 mm
Height	42.0 mm
Number of turns	84

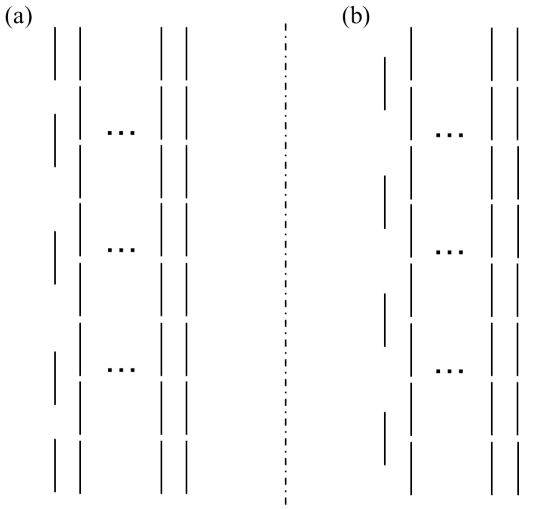

Figure 1. Cross-sectional views of axisymmetrical models for numerical calculations. (a) 85 strip loops (model 1) and (b) 84 strip loops (model 2)

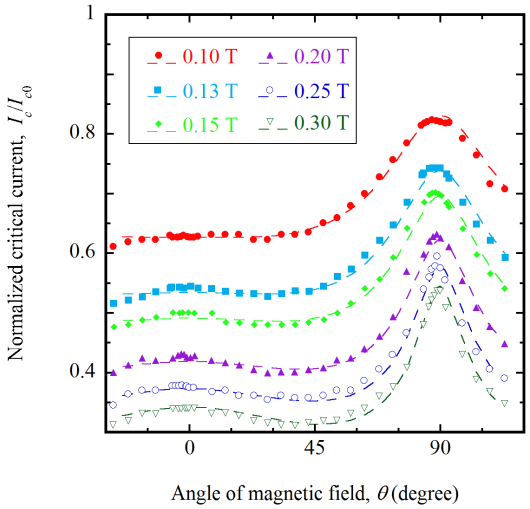

Figure 2. Comparison between experimental results [14] and approximate curves of critical currents in HTS tape.

and 70.7 mm, respectively. The height and turn number of coil are 42.0 mm and 84, respectively. Figure 1 shows the cross-sectional views of axisymmetrical models for numerical calculations, where two typical cross-sections of the HTS coil are considered. One is the cross-section drawn in figure 1(a) at which the current terminals are attached and there are 85 cylindrical SC strips, whereas the other is figure 1(b) in which we begin to wind the double pancakes and the number of strips is 84. The former and latter are called as models 1 and 2, respectively, in this study.

When we consider the current vector potential $\boldsymbol{T}$ defined by $\boldsymbol{J} = \nabla \times \boldsymbol{T}$ with the current density $\boldsymbol{J}$, the vector potential and current density in the cylindrical coordinate system (r, φ, z) have only the radial and azimuthal components as $\boldsymbol{T} = (T_r, 0, 0)$ and $\boldsymbol{J} = \left(0, J_\varphi, 0\right)$, respectively, which have a relationship given by $J_\varphi = \partial T_r / \partial z$, because the thickness d of the strip loop is much smaller than the width w. In this case, we can obtain the governing equation from Faraday's low as [1]

$$\frac{\partial}{\partial z}\left(\rho \frac{\partial T_r}{\partial z}\right) = \mu_0 d \frac{\partial}{\partial t} \sum_{j=1}^{N_e} F(r, z; r', z') \frac{\partial T_r}{\partial z'} \Delta z' + \frac{\partial B_{er}}{\partial t}, \tag{1}$$

where ρ is the resistivity of strip, N_e the total number of elements, which have the width $\Delta z'$ equal to one another, and B_{er} the radial component of external magnetic field. We consider that the self-field in the radial direction at the observation point (r, z) is generated by the current $\partial T_r / \partial z'$ flowing in the element, whose central coordinate is represented by (r', z'). Since the structure of equation (1) in the

cylindrical coordinate system is identical with that for the Cartesian coordinate system, we can use a program code for numerical calculations developed previously [12], except for the factor F determined by the geometrical arrangement of strips. The factor F in the cylindrical coordinate system can be expressed by [1]

$$F(r,z;r',z') = \frac{1}{4\pi}\frac{z-z'}{r}\frac{\sqrt{(r+r')^2+(z-z')^2}}{(r-r')^2+(z-z')^2}\left\{(2-k^2)E(k)-2(1-k^2)K(k)\right\}, \tag{2}$$

where $K(k)$ and $E(k)$ are the complete elliptic integrals of the first and second kinds, respectively, with the elliptic modulus k given by

$$k = \sqrt{\frac{4rr'}{(r+r')^2+(z-z')^2}}. \tag{3}$$

In the numerical calculations carried out in this study, the external field is always set to zero as $B_{er} = 0$. The governing equation (1) is discretized by means of the Galerkin method and backward difference method for space and time, respectively.

We use the critical state model (CSM) or n-value model (NVM) for the electric field vs. current density property in the SC strip. The resistivity ρ as a function of the local current density $J_\varphi = \partial T_r/\partial z$ for the CSM and NVM can be expressed by [13]

$$\rho(J_\varphi) = \begin{cases} 0, & \left|J_\varphi\right| \le J_c, \\ \rho_f\left(1-\dfrac{J_c}{\left|J_\varphi\right|}\right), & \left|J_\varphi\right| > J_c, \end{cases} \tag{4}$$

$$\rho(J_\varphi) = E_c\frac{\left|J_\varphi\right|^{n-1}}{J_c^n}, \tag{5}$$

respectively, where J_c is the critical current density and n is the n-value. The flux-flow resistivity ρ_f and the electric-field criterion E_c are set as $\rho_f = 1\times10^{-7}$ Ωm and $E_c = 1\times10^{-4}$ V/m, respectively. In order to take into account the dependence of critical current I_c at 77 K on the magnitude B and angle θ of applied magnetic field, the corresponding experimental results for a similar HTS tape [14] are approximated using the equation

$$\frac{I_c(B,\theta)}{I_{c0}} = \frac{\alpha_1 B^{-\Gamma_1}}{\sqrt{\cos^2\theta+\gamma_1^{-2}\sin^2\theta}} + \frac{\alpha_2 B^{-\Gamma_2}}{\sqrt{\gamma_2^{-2}\cos^2\theta+\sin^2\theta}}, \tag{6}$$

where the mathematical symbols, α_1, α_2, Γ_1, Γ_2, γ_1 and γ_2, are the fitting parameters given by $\alpha_1 = 0.0159$, $\alpha_2 = 0.0988$, $\Gamma_1 = 0.92$, $\Gamma_2 = 0.65$, $\gamma_1 = 1 + 19.4B$ and $\gamma_2 = 1 + 1.20B$ on the basis of the least squares method if the unit of field B is tesla. Figure 2 shows the comparison between the experimental results and approximate curves. The critical current density J_c in the SC strip as a function of field magnitude B and angle θ is expressed by $J_c(B,\theta) = I_c(B,\theta)/(wd)$. In the case of the Bean model [15], in which the critical current density is independent of the applied magnetic field, we use J_{c0} (= $I_{c0}/\{wd\}$) as a constant critical current density. Although the n-value also depends on the field magnitude and angle, we have no reliable information about the n-value in the present HTS tape. Therefore, we assume that the n-value has a property similar to the critical current as

$$\frac{n(B,\theta)-1}{n_0-1} = \frac{I_c(B,\theta)}{I_{c0}}, \tag{7}$$

where n_0 is the n-value at 77 K in self-field given by $n_0 = 35$ [14]. On the other hand, the n-value is fixed at n_0 for the case of constant n in the NVM. In the numerical calculations, it is assumed that all the discretized elements in an SC strip under consideration at each time step have an identical critical

current density and n-value represented typically at the center of the strip. Since the resistivity in the CSM or NVM has a strong non-linearity as can be seen in equation (4) or (5), the equation (1) is solved iteratively at each time step by means of the Newton–Raphson method.

The sweep rates of currents applied to the HTS coil are fixed at 1 A/s. When the transport currents become equal to the pre-determined values, the transport currents are held maximum. The SCFs B_{SCF} in the axial direction at the center of HTS coil, which is set as the origin of cylindrical coordinates, are estimated by two different methods as [1, 16]

$$B_{SCF} = \mu_0 \sum_{i=1}^{M} \frac{3 m_i r_i^2 z_i}{2\left(r_i^2 + z_i^2\right)^{5/2}}, \tag{8}$$

$$B_{SCF} = \mu_0 d \sum_{j=1}^{N_e} G(r', z') \frac{\partial T_r}{\partial z'} - B_0, \tag{9}$$

where M is the number of strips, m_i the radial magnetic moment per unit length in the i-th strip, (r_i, z_i) the coordinate at the center of the i-th strip, B_0 the ideal central field for the case where the currents uniformly flow over the strips and G the geometrical factor determined by the strip arrangement given by [1]

$$G(r', z') = \frac{1}{2}\left\{ \frac{z' + \Delta z'/2}{\sqrt{(r')^2 + (z' + \Delta z'/2)^2}} - \frac{z' - \Delta z'/2}{\sqrt{(r')^2 + (z' - \Delta z'/2)^2}} \right\}. \tag{10}$$

Equations (8) and (9) give us the numerical results identical to each other.

3. Calculated results

Figure 3 shows the comparison between the calculated results of SCFs for models 1 and 2 using the CSMs with constant J_c and $J_c(B, \theta)$. The HTS coils are monotonically energized from 0 A at the constant sweep rate of 1 A/s. In the case of the CSMs, the calculated electromagnetic fields are always in quasi-equilibrium, so that the instantaneous SCFs during the excitations for all the cases can be equal to the final values after the excitations are suddenly stopped. The experimental results of SCFs are also plotted with the symbols [11]. It can be seen in figure 3 that all the results including the experiments have a good agreement with one another in the cases of small applied currents. On the other hand, the discrepancies arize when the applied currents become larger, but the shapes of curves are almost similar to one another. This means that all the curves have a peak and the SCFs decrease with increasing the applied currents in their large range. It is also found that the differences between models 1 and 2 are very small and less than 7.4%. Therefore, the following calculated results are obtained only for model 1.

Figure 4 shows the time evolutions of SCFs during excitations up to 100 A and subsequent current holdings for three different transport properties in the SC strips. In the case of the CSM with $J_c(B, \theta)$, the SCFs during the excitation directly give us the steady-state calculated results as mentioned above. On the other hand, the calculated results of SCFs for the NVMs after the excitations ($t > 100$ s) gradually decrease with time due to the flux creep as shown in figure 4, and should become zero in the infinite time. In the experiments carried out previously, the readings of outputs from a Hall probe using a voltmeter to observe central magnetic fields in the order of 100 mT were carried out after first 4 digits of the output values became unchanged, which took roughly 1 minute [11]. This means that the measurement errors in the experimental results of SCFs shown in figure 3 were less than 0.1 mT. Therefore, we pick up the SCFs at three minutes after the excitations as the typical values of SCFs for the cases with the NVMs, whose magnitudes of time evolutions are less than 0.1 mT/min. The calculated results of SCFs after the excitations are plotted in figure 5, where three different transport properties in the SC strips are used. By using the NVM with $J_c(B, \theta)$ and $n(B, \theta)$, the obtained SCFs almost agree with the experimental results as can be seen in figure 5.

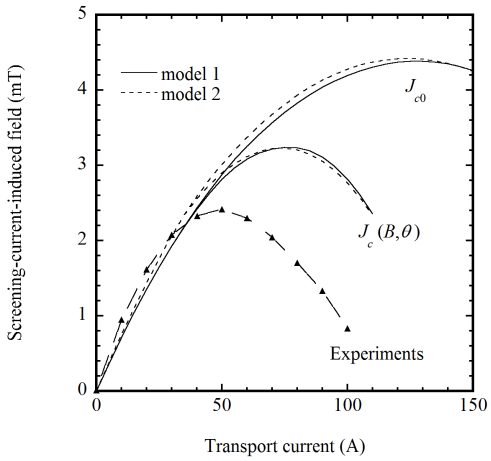

Figure 3. Comparison between calculated results of SCFs for models 1 and 2 using CSM. The symbols are the experimental results [11], and the broken line is a guide to the eye.

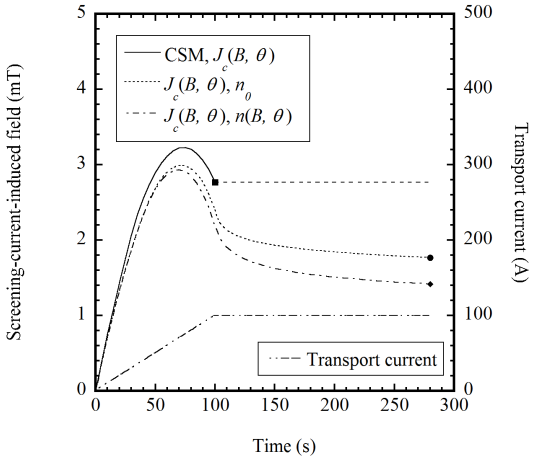

Figure 4. Comparison among time evolutions of SCFs during excitations up to 100 A and subsequent current holdings for three different transport properties in SC strips.

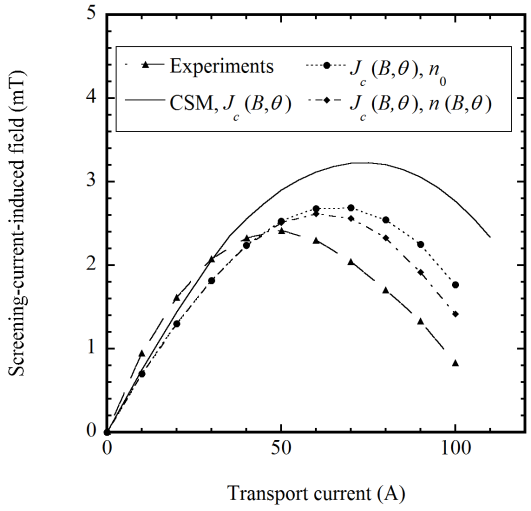

Figure 5. Comparison among calculated results of SCFs for three different transport properties in SC strips. The experimental results [11] are also plotted for comparison. The lines except for the solid line are a guide to the eye.

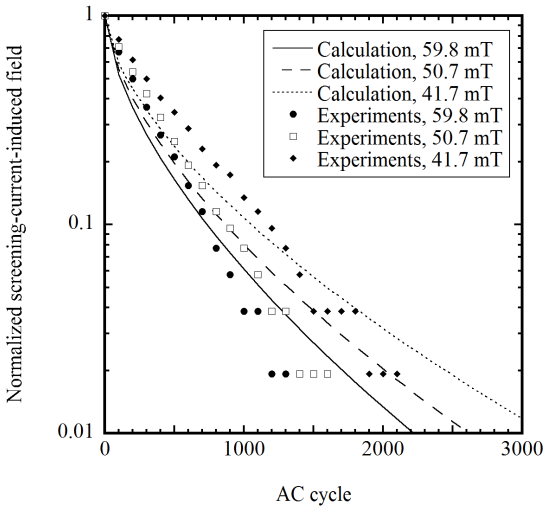

Figure 6. The decays of SCFs for applications of AC magnetic fields in azimuthal direction with three different amplitudes larger than full penetration field. The symbols show the experimental results [11], and the lines are the calculated results.

Figure 6 shows the decays of SCFs for the applications of AC magnetic fields in the azimuthal direction with three different amplitudes larger than the full penetration field of 32.1 mT. The symbols obtained in the experiments [11] are compared with the calculated results drawn using the curves, which are estimated in this study as follows. The critical current $I_c(B_i, \theta_i)$ in every strip after the excitation up to 100 A is obtained using equation (6), where B_i and θ_i are the magnitude and angle, respectively, of magnetic field applied at the center of the i-th strip. Then, the SCF B_{SCF} as a function of AC cycle N is

estimated using equation (8) with the magnetic moment m_i given by [7, 8]

$$m_i = m_0 \exp\left[-1.68\left(\frac{4B_m d}{\mu_0 I_c(B_i, \theta_i)}N\right)^{0.64}\right], \tag{11}$$

where m_0 is the initial radial magnetic moment per unit length in an SC strip loop under consideration after the excitation of the HTS coil and B_m the amplitude of AC field. The initial moment m_0 in every strip obtained from the finite element analysis using the NVM with $J_c(B, \theta)$ and $n(B, \theta)$ is used here. It can be seen in figure 6 that the experimental results are almost reproduced using the above-mentioned procedure for calculation.

4. Conclusion

The SCFs at the center of the HTS coil after initial excitations were numerically evaluated by means of the one-dimensional finite element method, where the CSM or NVM was used for the voltage-current characteristics of the SC strip loops. The NVM with the dependence of the critical current density and n-value on the magnitude and angle of applied magnetic field most closely reproduced the experimental results of SCFs carried out in the previous work. The applications of the existing theoretical expression for the single strip to all the turns with the separate critical currents and initial magnetic moments obtained from the numerical calculations almost agreed with the experimental results on the decays of SCFs in the HTS coil exposed to the azimuthal AC magnetic fields.

References

[1] Amemiya N and Akachi K 2008 *Supercond. Sci. Technol.* **21** 095001
[2] Funaki K and Yamafuji K 1982 *Japan. J. Appl. Phys.* **21** 299
[3] Funaki K, Niidome T and Yamafuji K 1982 *Japan. J. Appl. Phys.* **21** 1121
[4] Funaki K, Noda M and Yamafuji K 1982 *Japan. J. Appl. Phys.* **21** 1580
[5] Funaki K, Niidome T and Yamafuji K 1983 *Tech. Rep. Kyushu Univ.* **56** 45
[6] Brandt E H and Mikitik G P 2002 *Phys. Rev. Lett.* **89** 027002
[7] Mikitik G P and Brandt E H 2003 *Phys. Rev. B* **67** 104511
[8] Brandt E H and Mikitik G P 2004 *Supercond. Sci. Technol.* **17** S1
[9] Kajikawa K and Funaki K 2011 *Supercond. Sci. Technol.* **24** 125005
[10] Kajikawa K and Funaki K 2012 *IEEE Trans. Appl. Supercond.* **22** 4400404
[11] Kajikawa K and Okabe Y 2016 *IEEE Trans. Appl. Supercond.* **26** 4400504
[12] Kajikawa K, Mawatari Y, Iiyama Y, Hayashi T, Enpuku K, Funaki K, Furuse M and Fuchino S 2006 *Physica C* **445–448** 1058
[13] Kajikawa K, Hayashi T, Yoshida R, Iwakuma M and Funaki K 2003 *IEEE Trans. Appl. Supercond.* **13** 3630
[14] Daibo M, Fujita S, Haraguchi M, Iijima Y, Itoh M and Saitoh T 2012 *IEEE Trans. Appl. Supercond.* **22** 3900204
[15] Bean C P 1962 *Phys. Rev. Lett.* **8** 250
[16] Kajikawa K, Gettliffe G V, Chu Y, Miyagi D, Lécrevisse T P, Hahn S, Bascuñán J, and Iwasa Y 2015 *IEEE Trans. Appl. Supercond.* **25** 4300305